This article has been accepted for publication in a future issue of this journal, but has not been fully edited. Content may change prior to final publication. Citation information: DOI 10.1109/TSTE.2018.2849370, IEEE Transactions on Sustainable Energy

A 3-D Pareto-Based Shading Analysis on Solar Photovoltaic System Design Optimization

Pedram Asef, *Student Member, IEEE,* Ramon Bargallo, M. R. Barzegaran, *Member, IEEE* and Andrew Lapthorn, *Member, IEEE*

***Abstract*— This paper utilizes a Pareto-based, three-dimensional (3-D) analysis to identify complete and partial shading of photovoltaic (PV) systems for an complicated urban environment, where unusual shape of PV and installation topology is studied. The Pareto optimization attempts to minimize losses in a certain area with an improved output energy and without compromising the overall efficiency of the system of which, the nominal operating cell temperature (NOCT) for a glass/glass-module is considered as a significant parameter. The system is referenced to the environment based on IEC61215 via a closed-circuit and resistive load to ensure the module operates at the maximum power point. A Maximum Power Point Tracking (MPPT) controller is enhanced with an advanced perturb and observe (P&O) algorithm to maintain the PV operating point at its maximum output under various working conditions. The most cost-effective design of the PV module is achieved via optimizing installation parameters such as tilt angle, pitch, and shading to improve the energy yield. The parameter settings and suitability of the design are also determined based on the reduced amount of CO2 emissions. An experimental investigation has been carried out to verify the 3-D shading analysis and NOCT technique for both open-circuit and grid-connected PV modules.**

***Index Terms*—Photovoltaic System, Three-Dimensional Shading Analysis, Pareto Optimization, Partial Shading Analysis, Perturb and Observe Algorithm, Window-Zoom-in.**

I. INTRODUCTION

SUSTAINABLE energy and technology development plays a significant role in power generation today. Photovoltaic (PV) system design and development has been combined with advanced shading analysis to predict and enhance the output power and losses resulting from complete and partial shading. The shading effect evaluation, with any level of variation, is essentially a mechanical design aspect but directly affects the main electrical factors. A PV module depends on a photovoltaic cell, which generates an electrical current when solar radiation strikes its surface. The operation and performance of a PV module is affected by various factors such as; solar radiation, ambient temperature, PV array configuration and shading, which may be either complete or partial. A partial shadow can be caused by clouds, trees, neighboring buildings and utilities. The shadow effect causes the output power and efficiency to decrease and a high power loss in the shaded cells producing a hot spot [1-2].

A paper by Zhen *et al.* [3] presents valuable research on the nominal operation cell temperature (NOCT) under the IEC61215 standard for building-integrated photovoltaic (BIPV) modules. The authors found that the measurement error on a simulated BIPV house was about 15°C higher than that of modules on an open rack. This is a considerable difference and more accurately resembles the conditions under which the modules would be used. It is important to determine the NOCT of BIPV modules by measuring it in the simulated BIPV house. A 7°C temperature difference was found between grid-connected and open-circuit modules. Thus, the NOCT has to be tested under closed-circuit condition to better mimic the real operating conditions of the modules. In this study, we have tested the PV module in both grid-connected and open-circuit experiments to evaluate and verify this fact.

N. Belhaouas *et al.* [4] presents three new physical PV array arrangements, which are proposed to mitigate partial shading effects. The arrangements are based on maximizing the distance between adjacent PV modules within a PV array by appropriately arranging modules in different rows and columns without changing the electrical connections. A systematic analysis is performed to assess the proposed PV array arrangements. The new configurations simplify operation and improve performance significantly compared to the reference Series-Parallel (SP) and Total Cross Tied (TCT) configurations. The characteristic power-voltage curves exhibit a single peak allowing tracking of the maximum power point with a simple controller removing the need for complex controller algorithms and costly hardware, and the power output gains range from 19 to 140% compared to SP, and 13 to 68% compared to TCT.

R. Rachchh *et al.* [5] propose a novel approach to maximize the total number of solar panels in a given area with an enhanced energy output without compromising the overall efficiency of the system. The number of solar panels can be maximized in a solar PV energy generation system by optimizing installation parameters such as tilt angle, pitch, gain factor, altitude angle and shading to improve the energy yield. In their paper, a mathematical analysis is performed to prove that the capacity and generated energy can be enhanced by more than 25% for a given land area through optimization of various parameters under different shading patterns and scenarios, and to compare the performance with existing configurations.

Pedram Asef, and Professor Ramon Bargallo Perpina are with the Department of Electrical Engineering, Polytechnic University of Catalonia-BarcelonaTech, Campus Diagonal-Besòs, 08019 Barcelona, Spain, (e-mail: pedram.asef@upc.edu; ramon.bargallo@upc.edu).

Dr Barzegaran is Assistant Professor and Director of Renewable energy Microgrid Laboratory at Lamar University (A Texas State University), TX, USA (email: barzegaran@lamar.edu).

Dr. Andrew Lapthorn is a Senior Lecturer at the Department of Electrical and Computer Engineering, University Of Canterbury, Christchurch, New Zealand (email: andrew.lapthorn@canterbury.ac.nz).

This article has been accepted for publication in a future issue of this journal, but has not been fully edited. Content may change prior to final publication. Citation information: DOI 10.1109/TSTE.2018.2849370, IEEE Transactions on Sustainable Energy

In another paper [6], the authors introduce a Pareto-based design-optimization problem solver for designing new energy-efficient static daylight devices that surround the external windows of a residential building in Madrid. The study identified, via a multi-objective optimization methodology, the set of optimal shading devices that allow low energy consumption of the dwelling while maintaining high levels of thermal and lighting comfort for the inhabitants.

In [7], A. J. Hanson, *et al.* demonstrate the measured performance data at the module level for 542 PV systems to estimate the lost system performance due to partial shading. They have improved by an average of 36% of the power lost due to partial shading via use of module-level dc power electronics.

In this research, we investigate the influence of complete and partial shading on an annual basis using 3-D dynamic shading analysis for an application-oriented design in a new urban environment (Fig. 1). An analysis of variance (ANOVA) method using un-replicated factorials via a dual-level window-zoom-in approach was used to determine the dominant design factors over three design variables while under various rates of shading. The focus is on the input data (i.e. NOCT, weather and sky condition data, and ambient temperature) that have a direct effect on the module's outputs. The aim is to minimize the number of shaded cells and consequently maximize the output power of the system as a whole. A maximum power point tracking (MPPT) method, enhanced by a Perturb and Observe Algorithm (P&O) was, employed to reach the maximum possible output power. The proposed technique uses Pareto optimization, which relies on the input weather data. In section III, a 3-D shading analysis design and optimization technique is introduced and discussed where the procedure and methodology used are one of the main contributions of the paper. The results and discussion (Section IV) present the numerical outcomes of the work, which is verified in Section V. Finally, the work's contributions and achievement are concluded in Section VI.

II. Analytical Modeling and Data Acquisition

Fig. 1(a) shows that the tower, as a part of an application-oriented renewable energy system design for power generation, consists of eight branches in the direction of suns' track where the *x*-axis and *y*-axis present the east and north directions, respectively. A total area of 30 m^2 is reserved for the PV cells,

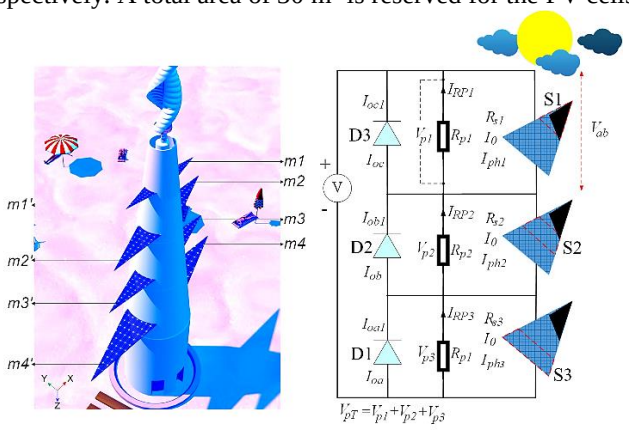

(a) (b)

Fig. 1 3-D modelling and equivalent circuit of a PV module with shading

where each PV module (Fig. 1(b)) is presented as module $m1$ in series with module $m1'$. The PV system is designed with four series and parallel connections. An equivalent circuit of a PV module is simplified into three cells in series with three bypass diodes. V_{pT} is the total terminal voltage of the shaded cells, which is acquired via summation of V_{p1}, V_{p2} and V_{p3}. These voltages are across R_{p1}, R_{p2}, and R_{p3} due to shaded cells. The shading analysis is studied for one of the branches, which has approximately 60 cells. The S1, S2, and S3 areas have 24 cells each for the top, middle, and bottom sections of the module, respectively. The parameters of these three cells' areas and diodes are assumed variable due to shading. In addition, the bypass diodes are shut down only if the three cells are receiving equal irradiation. Based on the commonly employed single diode solar cell model, the output current I by the load is given through Eq. (1) [8-10]:

$$I = I_{ph} - I_0\left(\exp\left[\frac{q.(V + IR_s + I_{RP1}R_{p1} + I_{RP2}R_{p2} + I_{RP3}R_{p3}}{A.k.T}\right] - 1\right) \quad (1)$$

I_{ph} and I_0 are the photocurrent and the inverse saturation current, respectively. R_s is the total series resistance (which is summed by $R_s = R_{s1} + R_{s2} + R_{s3}$). A is the ideality factor of the diode. T shows the ideality factor of the temperature in Kelvin. q is electron charge 1.6×10^{-19} C and k is Boltzmann's constant 1.38×10^{-23} J/K. The partial shading causes voltage drops of V_{p1}, V_{p2}, and V_{p3} which originate from R_{p1}, R_{p2}, and R_{p3}. Hence, each area of the module (S1, S2, and S3) passes the currents of $I_{R_{P1}}$, $I_{R_{P2}}$, and $I_{R_{P3}}$, respectively.

The current I_b that passes the bypass diode can be calculated from:

$$I = I_{ob}\left(\exp\left[-\frac{q.V}{A_b.k.T_b}\right] - 1\right) - \frac{q - V}{R_p} \quad (2)$$

For example, I_{ob} is calculated by (photo current (I_{ph}) – saturation current (I_{Sat})) of each S1, S2, and S3 areas, in which I_{ph} is linearly dependent on the irradiance and increases with increasing cell temperature [10]:

$$I_{ph}(n) = \sum_{n=1}^{3}(C_1 + C_2.T_n)E_n \quad (3)$$

In this study, I_{ph} is calculated for $n = 1$, 2, and 3 due to the module cells segmentation (S1, S2, S3). C_1 and C_2 are cell-dependent parameters, T_n is the temperature measured on each segment by an infrared thermal camera for different conditions, E_n is the global radiation onto segment area.

The saturation current is defined in this research as:

$$I_{Sat}(n) = \sum_{n=1}^{3} C_s T^{k_n} \exp\left(-\frac{E_{gap}(n)}{m.k_n.T_n}\right) \quad (4)$$

where C_s is a material and technology-dependent constant ($C_s = 10^2$), k is the exponent of the temperature which is normally defined as $k = 3$ in the literature. $E_{gap}(n)$ is the band gap of the cell material which is functional to each segment temperature. For instance, $E_{gap}(3)$ at a measured temperature of 26˚C is approximately equal to 1.13 eV for silicon [10].

The parallel resistances (R_{p1}, R_{p2}, and R_{p3}) are inversely proportional to the irradiance which is computed for various shading levels, while the series resistances (R_{s1}, R_{s2}, and R_{s3})

This article has been accepted for publication in a future issue of this journal, but has not been fully edited. Content may change prior to final publication. Citation information: DOI 10.1109/TSTE.2018.2849370, IEEE Transactions on Sustainable Energy

are negligible for irradiance and temperature changes. Consequently, the influence of shading on R_p is significant and one of the major factors to be considered in this research.

$$R_p(E_n) = \sum_{n=1}^{3} R_p \frac{E}{E_n} \tag{5}$$

under short circuit condition, R_p (total parallel resistance) and E have been specified, however E_n is the segment-dependent radiation in the PV module. n reflects to the module's sections which can be either 1, 2, or 3.

$$\begin{aligned}
&if \quad I_{ph1} < I < I_{ph2}: \\
&V_i = \frac{AkT}{q}\ln\left(\frac{I_{ph2}-I}{I_0}+1\right) - \frac{A_b.k.T_b}{q}\ln\left(\frac{I-I_{ph1}}{I_{ob}}+1\right) - IR_s - IR_p \\
&if \quad I_{ph2} < I < I_{ph3}: \\
&V_j = \frac{AkT}{q}\ln\left(\frac{I_{ph3}-I}{I_0}+1\right) - \frac{A_c.k.T_c}{q}\ln\left(\frac{I-I_{ph2}}{I_{oc}}+1\right) - IR_s - IR_p \\
&if \quad 0 < I < I_{ph1}: \\
&V_k = \frac{AkT}{q}\ln\left(\frac{I_{ph1}-I}{I_0}+1\right) - \frac{A.k.T}{q}\ln\left(\frac{I_{ph2}-I}{I_0}+1\right) - 2.IR_s - IR_p
\end{aligned} \tag{6}$$

With respect to Fig. 1, a shadow falls on cell number 1 which results in an energy input reduction to the cell. The energy loss at the partially shaded cell is increased when cell number 2 is connected and completely under illumination (i.e. no shadow). The photocurrent, I_{ph2}, is seen to be higher than that of the shaded cell, I_{ph1}.

The output characteristics of the partially shaded PV module are different from those of the completely illuminated module due to the decreased luminous energy input. In addition, because of the existence of a bypass diode, as illustrated in Fig. 1, the shaded cell is protected from damage by hot spots. The *I-V* curve of the partially shaded PV module is defined through a piecewise function (Eq. 6) that breaks at the state switching point of the bypass diode. Three states are defined to predict the voltage drops (V_i, V_j, and V_k) based on the current variation due to the various shading factors on each section of the module.

Using the equivalent model in Fig. 1(b), the shading analysis of the PV module is theoretically acquired where a PV module containing N solar cells is divided into K groups via connecting K bypass diodes in parallel ($N \geq K$, not overlapping). If shadows fall on the solar cells at various proportions for each group, a voltage drop will affect the *I-V* curve and consequently output power of the PV module, which is presented in K steps [9-10].

In PV systems, data acquisition plays a major role due to different weather dependent factors such as the sun's height based on the azimuthal map, the modules' temperature, and shading obstacles. These databases are stored using numerical and experimental methods for a high accuracy computation.

A. Weather Data Acquisition and Investigation

In this original study, the horizon shading is modelled as abroken line superimposed onto the sun path diagram, which can hold any number of height/azimuth points. The horizon profile is designed using *PVsyst* and *PV*Sol* software for a specific location on the Barcelona coast in Spain. In addition, the meteorological data regarding at the location of the project is considered. Fig. 2 illustrates the simulated annual horizon line of the target location where the PV modules are installed. During azimuth = 0˚, at approximately 13:00, the height of the sun can be between 74˚ to 79˚ in the peak days of the year (May, June, and July).

This study uses two major parameters for the output power prediction. First, the nominal operation cell temperature (NOCT) found using the method studied in [3]. Then, the solar irradiance to the tilted surface of the PV generator is predicted while considering complete or partial shading of the module.

The active solar surface gives the radiation to the horizontal plane (in W/m^2). According to the DIN5034-2 standard, the tilted global irradiance onto the PV modules, based on geometric principles, is calculated using:

$$\mathrm{E}_{G,t} = \mathrm{E}_{Dir,t} + \mathrm{E}_{Diff,t} + \mathrm{E}_{\mathrm{Re}f,t} \tag{7}$$

where $E_{Dir,t}$, $E_{Diff,t}$, and $E_{Ref,t}$ are the tilted parameters of the direct and diffuse components of the solar irradiance onto the horizontal plane, and the reflected radiation from the ground, respectively.

Fig. 3 represents carpet plots with a consideration of radiation and temperature distribution on the PV module area, where Fig. 3(a) shows how the global radiation appears on the module, and Fig. 3(b) illustrates deviation from the nominal module temperature. The boundary of radiation onto the tilted active PV surface, which varies between 8:00 to 16:00 (shown in Fig. 3(b)), is slightly smaller than the global radiation on the module (06:00 to 19:00) shown in Fig. 3(a). In Fig. 3(b), the deviation exists mainly during the night, during fully cloudy hours between -25 to 18 W/m^2, and much less during the day time (09:00 to 16:00) with the variation of -60 to -280 W/m^2.

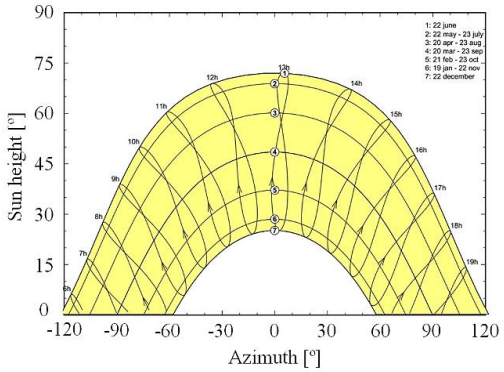

Fig. 2 Annual horizon condition in the targeted area based on horizon line

B. Maximum Power Point Tracking (MPPT) Based on a Perturb and Observe (P&O) Algorithm

The conventional algorithm of perturb and observe (P&O) has been widely applied because of its simplicity, low cost and easy implementation [11-14]. However, it suffers from instabilities during rapid changes of weather and/or oscillation around the maximum power point (MPP) under a steady-state condition, which is a major concern of this research. Hence, a modified- P&O algorithm, which has been validated in [12] is used for the following improvements: (1) convergence time reduction, (2) continuous perturbation, and (3) tradeoff between step sizes.

This article has been accepted for publication in a future issue of this journal, but has not been fully edited. Content may change prior to final publication. Citation information: DOI 10.1109/TSTE.2018.2849370, IEEE Transactions on Sustainable Energy

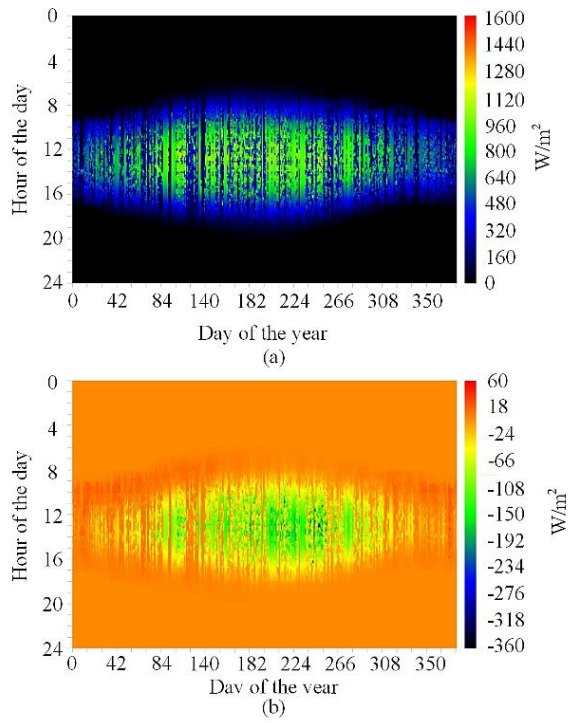

Fig. 3 Annual simulation of PV module's observation for: (a) the global radiation onto the module, and (b) deviation from the nominal module temperature

The formulation of the MPPT used, based on the DC- DC buck converter, are given as:

$$V_{out}(d) = V_{pv} \times d \tag{8}$$

$$I_{out}(d) = \frac{I_{pv}}{d} \tag{9}$$

$$d = \frac{1}{(1-d')} \tag{10}$$

$$S_L(d) = d^2\left(\frac{I_{out}(d)}{V_{out}(d)}\right) = \frac{d^2}{R_L} \tag{11}$$

$$R_L(d) = d^2\left(\frac{V_{pv}}{I_{pv}}\right) \tag{12}$$

where V_{out} and I_{out} are the output voltage and current of the DC-DC converter as a function of d which is a linear control variable between V_{out} and V_{pv}. d' is the duty cycle of the converter. S_L is the slope of the load line, and R_L is the output load resistance of DC-DC converter [15].

There are a number of studies on PV module optimization using different methods (such as [16-18]). Regarding the above equations between the input and output variables of the DC-DC buck converter, the following problem formulation can be studied for the Pareto optimization:

$$\begin{cases} Maximize: P_{eff}(z) \\ Subjected: \quad z_{\min} \le z \le z_{\max} \\ z_i = z_{i-1} \pm \phi \quad if \quad P_o > P_{o,i-1} \end{cases} \tag{13}$$

$P_{eff}(z)$ is the PV array's effective output energy where z is duty ratio of the DC-DC converter. The lower (z_{min}) and upper (z_{max}) limits of the duty ratio are from 5% to 95%, respectively. Under the perturbation setting of the optimization, the new duty ratio (z_i) has to provide a faster convergence and higher steady-state oscillation, only if the perturbed duty cycle (ϕ) has a large value. Whereas, smaller ϕ costs the system's convergence with slower performance. Hence, the new and larger output power (P_o) is considered to be larger than those last tracked points $(P_{o,i-1})$.

III. Configuration Layout For Shading Analysis and Optimization

This section details the methodology used and simulation results for the PV modeling and power electronic software, based on sorting of data via a design of experiment (DOE) utilizing a full factorial function [19]. The following procedure is used to verify the dynamic performance, annual weather observation, complete and partial shadings, P&O algorithm for MPPT, and power electronics:

Step 1 Storing weather condition data such as module temperature and defining the presence of the clouds for 0%, 20%, 40%, 60%, 80% and 100% (normal) during months of January (minimum power generation) and June (maximum power generation).

Step 2 Initialize major design parameters such as pitch, and tilt for a variation of the capture beam, sailing, and optical losses. Afterwards, the zoom-in-window approach based on ANOVA, is employed to find the optimum values to minimize the losses and shading rate over a single 60 cell module.

Step 3 A conventional P&O algorithm is also simulated and compared to the proposed one (shown in Fig. 4) in order to highlight improvements. In addition, a model for the shading rate of a module is used in a Simulink environment utilizing *Step* (*1*) data for maximizing the power through the MPPT method. The MPPT uses the proposed P&O algorithm due to a number of advantages for this study.

Step 4 Execute the whole system, and store the output data for each day of the targeted months.

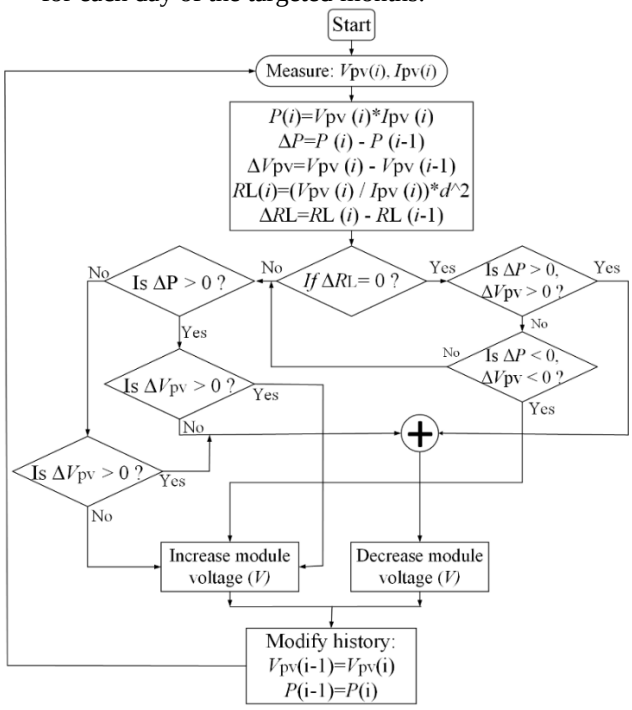

Fig. 4 The modern P&O algorithm used for the maximum power point tracking

This article has been accepted for publication in a future issue of this journal, but has not been fully edited. Content may change prior to final publication. Citation information: DOI 10.1109/TSTE.2018.2849370, IEEE Transactions on Sustainable Energy

For the simulation studies, the parameters of the PV module are given as: $P_{max} = 150$ W, $V_{mp} = 18.2$ V, $I_{mp} = 8.34$ A, $V_{oc} = 21.6$ V, $I_{sc} = 9.17$ A with a power tolerance of 3%.

The complete shading depends on four major factors, the horizon of the environment, pitch, tilt, and obstacles. Dynamic modeling via a time domain software package is sufficiently able to estimate the losses caused by this type of shading. Whereas, partial shading requires more data to enable a prediction. For this problem, the amount of cloudy hours for the targeted months is stored for a fast prediction. In addition, a power electronic-based simulation is completed where a 60 cell module splits off equally to three cell parts (S1, S2, and S3 in Fig. 1). Any voltage drop because of large R_p in one of those parts indicates larger shading losses (including complete and partial) over that number of cells.

For the 3-D structure of the project, *Google sketchUp 8* was used analyze the three-dimensional model environment geometry and to read information such as latitude, longitude, date and time. This information and the sky condition data, when introduced in *PVsyst*, allows for the estimation of the effective irradiation and the shading factor for a selected surface in the three-dimensional model, shown in Fig. 5 in which each branch holds PV modules. *PVsyst* software evaluated the shading analysis for a whole year.

The design and optimization procedure of the study is presented in Fig. 6. The flowchart is presented in two parts. Firstly, with the pre-calculation procedure which is shown on the left side. The right side of the flowchart represents the optimization process which is linked to the stored output data. ANOVA for un-replicated factorials based on a DOE is employed to check the accuracy where $X1$, $X2$, and $X3$ are the controllable variables pitch (P), tilt angle (β), and NOCT of the PV module. The main objective of the study is the maximization of the output power which depends on a number of design factors, particularly the shading analysis to decrease the total shading factor (S_t), where $S_t = S_c$ (complete shading) + S_p (Partial shading). Equation (13) can be maximized when the optimum values for the variables (shown in Table I) are found in the original design region. A modern P&O algorithm (MPPT) was used to trace the peak values for voltage, current, and power under a number of conditional terms defined as the design region (conditional optimization in Fig. 6). The optimization loop continues until the minimum total shading is achieved, and consequently, the $P_{eff}(z)$ value is maximized.

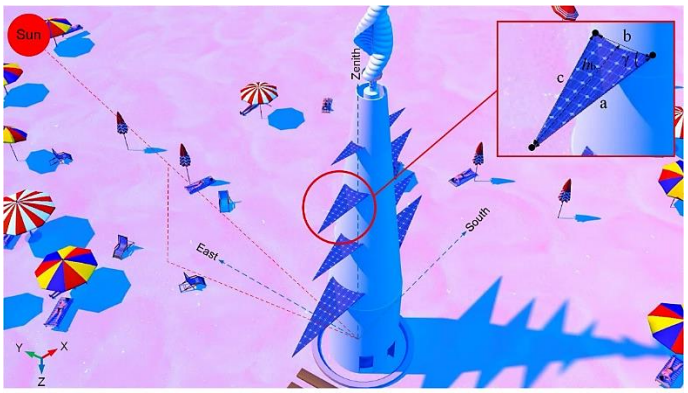

Fig. 5 The three-dimensional model environment for shading analysis

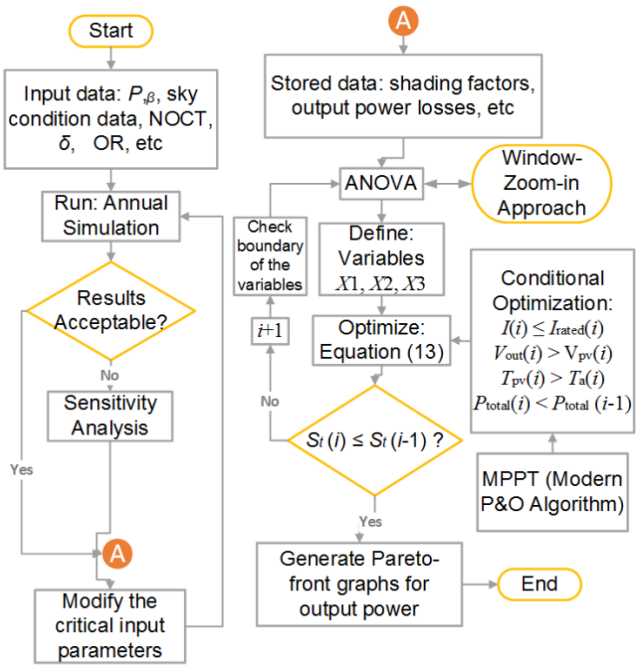

Fig. 6 The numerical-based methodology scheme

Table I. ORIGINAL DESIGN CONTROLLABLE VARIABLES

Controllable design treatments		*Coded design treatments*		
All variables are normalized		-1	0	1
x_1	Pitch length (m), P	0.5	1.5	2.5
x_2	Tilt angle (˚), β	10	30	50
x_3	Height of the branch (m), h_b	1	4	7

For this target, the window-zoom-in approach was utilized for a more accurate design using a 2nd -level design region for the variables. 24 variable data were analyzed, the optimum operation point was achieved in the second level plane where the output power is maximized and beam and shading losses are minimized.

IV. RESULTS AND DISCUSSION

To develop the proposed methodology, the following software has been utilized, *Google SketchUp 8*, *PV*Sol Pre.2017*, *PVsyst Ver*. 6.66, and *Matlab Simulink R17a* to perform the three-dimensional model.

In this study, two main simplifications are used which do not affect the concept and performance accuracy. To reduce the data's volume, the results are considered only for two months, June (peak operation time) and January (minimum operation time) in order to decrease the volume of data. The complete and partial shading analysis were simulated and verified only for one branch (all the other branches could be analyzed by the same computation procedure and optimization methodology used). The shading analysis on the branch marked in Fig. 5 was modelled.

Fig. 7 illustrates the output power behavior using the optimum vales of $X1$, $X2$, and $X3$ under different radiation rates to evaluate unexpected fluctuating zones through sudden changes in the input data (solar radiation). At radiation rates of 400, 600, and 1000 kW/m^2, an output power of 56, 65, and 129 W were achieved with an acceptable performance by the modern P&O algorithm. The conventional P&O algorithm contained much higher fluctuations especially under the

This article has been accepted for publication in a future issue of this journal, but has not been fully edited. Content may change prior to final publication. Citation information: DOI 10.1109/TSTE.2018.2849370, IEEE Transactions on Sustainable Energy

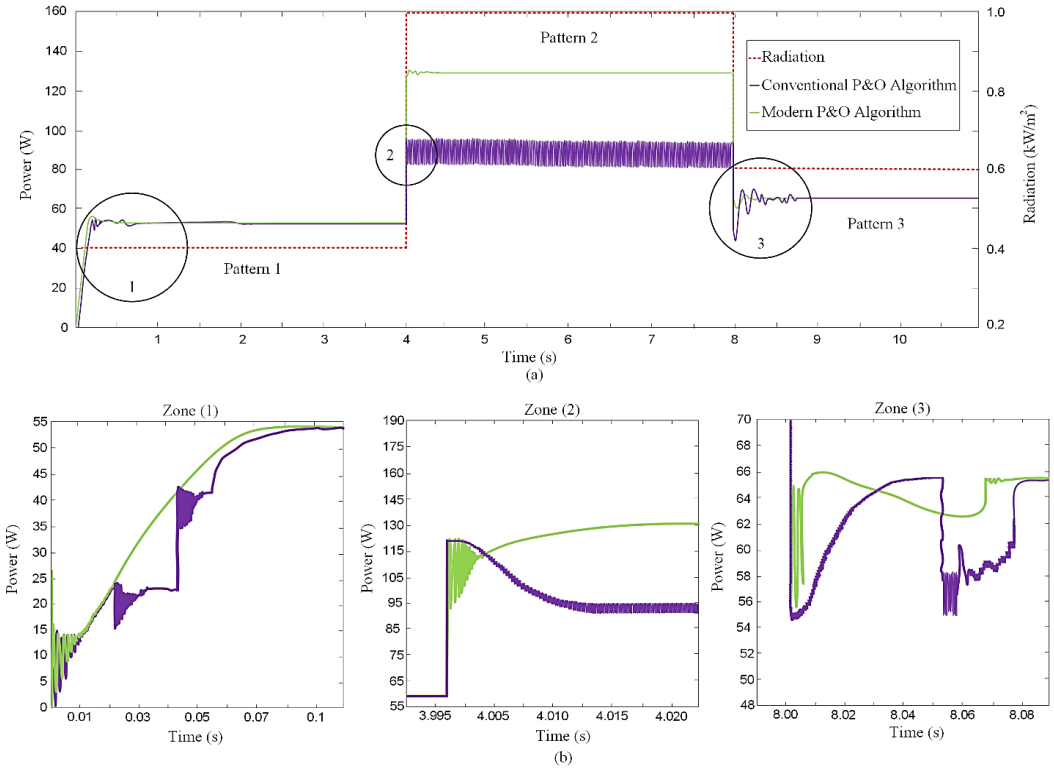

Fig. 7 The maximized output power using conventional and modern P&O algorithms for different radiation condition in the simulation, where a) presents the resilient spectrum of a complete 10s simulation, in which three patterns are considered with 400, 600, and 1000 kW/m^2, b) represents a zoomed in view during condition switching period of time

1000 kW/m^2 simulation condition. Fig. 7(a) zone (1) shows how the modern MPPT controller has improved the output power with a faster convergence. In zone (2), a significant voltage drop exists which leads the power to a 15 W peak to peak non-stabilized variation (shown in Fig. 7(b)). In zone (3), the power achieved a steady-state after 1 second of oscillations. The modern P&O algorithm performs well during any unexpected and quick weather condition changes compared to the conventional type.

Table II presents the second-level variation of responses (y_i) for the optimum variable values as $X1 = 1.51$ (pitch length), $X2 = 31$ (tilt angle), and $X3 = 5.6$ (height of branch), where DF is the degree of freedom, SS is the sum of squares, MS is mean square. The fitted regression model was checked via an F-value statistic to ascertain the validity of the null hypothesis. Also, the P-value is a significant non-zero value, which is the probability of rejecting the factor, interaction, or blocking BASED ON ITS F-VALUE STATISTIC.

Table II.

THE SECOND LEVEL ANOVA OF DOE WITH 5% LEVEL

Source of Variation	y_i	*DF*	*SS*	*MS*	*F-*	*P-*
Regression		3	33.285	33.285	5.194	0.097
Residual	P_o	4	25.631	6.408	-	-
Total	[W]	7	58.917	-	-	-
Regression		3	0.313	0.313	0.304	2.31
Residual	P_s	4	4.125	1.031	-	-
Total	[W]	7	4.439	-	-	-
Regression		3	1.103	1.103	1.446	1.662
Residual	P_b	4	3.055	0.764	-	-
Total	[W]	7	4.159	-	-	-
Regression		3	161.506	161.506	7.336	0.865
Residual	GlobEff	4	88.059	22.015	-	-
Total	[kWh/m^2]	7	249.565	-	-	-
Regression		3	1.583	1.583	3.993	1.633
Residual	E_{array}	4	1.586	0.397	-	-

Fig. 8(a) presents the variation of *I-V* curves where the shading cells factors are 20%, 40%, 60%, 80%, and 100% (normal) for the months of January and June with average ambient temperatures of 10 and 24˚C, respectively. The uniform and dashed lines show the results during January and June for shading factors of 100%, 80%, 60%, 40%, and 20%, respectively. A power reduction up to 10 W between -

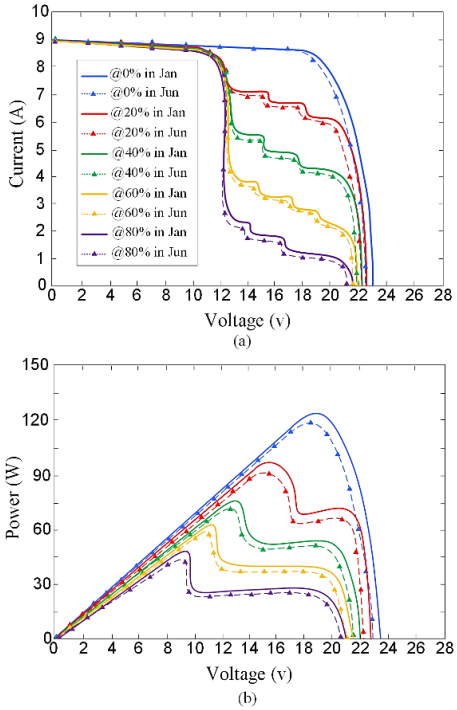

Fig. 8 The monthly PV module's outputs for different shading factors with respect to T_{amb} and rate of shaded cells: a) I-V variation, and b) P-V spectrum

This article has been accepted for publication in a future issue of this journal, but has not been fully edited. Content may change prior to final publication. Citation information: DOI 10.1109/TSTE.2018.2849370, IEEE Transactions on Sustainable Energy

-the two months can be seen due to the power loss from the ambient temperature.

The influence of the shading analysis with respect to the input data (sky) has direct effect on the R_p which correlates to the shaded cell rate, and thus any voltage drop over R_p results in the *I-V* and *P-V* variations shown in Fig. 8. The simulation was done on one PV module of 60 cells using two databases under open-circuit conditions. First, the weather and sky data are simulated using *PVsyst* and *PV*Sol* software as input data to the power system part of the analysis, simulated with *Simulink*.

Fig. 9 presents generated Pareto-front graphs for the effective energy at the output of the array during two months (winter/ and summer). The values spectrum shown in Fig. 9(a) during the month of January indicated an average available energy of 2.7 kWh/day, in which the extracted output power and its relative module power losses are compared for different shading factors in Fig. 9(b). Under partial shading conditions, the relative module power losses (including beam loss) are defined as $\%\Delta P_{RL} = [P_o - P_s/P_o\,] * 100$, in which P_o is the maximized output power of the PV array, and P_s is the maximized output power of the partially shaded PV array. $\%\Delta P_{RL}$ was reduced while the highest possible power is reached with the G = 1000W/m^2 condition. Fig. 9(c) illustrates the values of effective energy of the array for June where an average of 3.3 kWh/day was noted. For similar conditions, the extracted output power and relative power losses are computed and shown in Fig. 9(d). Much lower losses and higher output power were delivered in June compared with January.

Table III depicts the major design parameters of a 30 m^2 cell area before (original plane) and after the optimization (second level plane) in January and June, where the shading factor is considered. The simulation is carried out with a grid-connected (closed-circuit) condition, instead of only using open-circuit NOCT values. Thus, the NOCT are accurately calculated and are slightly reduced post-optimization. Under partial shading conditions, the first affected parameter is V_{pT} which increases when R_{p1}, R_{p2}, and/or R_{p3} (total value of R_{pT}) have risen. The parameter was calculated for different shading factors and has been considerably mitigated. Under each shading factor, V_{pT} is optimized at approximately 0.045 V. The GlobEff (or effective global irradiation of the collectors), which also has a direct relation with shading, was significantly raised by an average value of 25 kWh/m^2 through the proposed optimization. E_{array} (energy produced by the PV array) is another significant parameter which is influenced immediately after shading occurs. The produced energy has been maximized with an average of 5.5 kWh. P_{lossm} is the total minimum power losses caused by the shading and beam losses, for instance (in June), P_{lossm} (100%) = 0.2952 W is optimized to 0.2935 W. Finally, the objective defined in Eq. (6) is sufficiently satisfied where about $P_o = 30$ W maximization is apparent at various levels of shading.

V. Experimental Investigation

This section not only verifies the numerical analysis, but also provides the input data such as ambient temperature, sky data (clouds), and NOCT. The PV system which was tested is summarized in Table IV.

Fig. 10 illustrates infrared thermography of the tested glass/glass PV module under grid (closed-circuit) and open-rack conditions. The experiment shows that there is a considerable difference in the module's surface when the module is connected to the grid as shown in Fig. 10(a). The difference varies between 5 to 10˚C (G = 1000 W/m^2) depending on the experiment test type, module characteristics and weather condition. Fig. 10(b) presents a 5˚C lower temperature due to having an open-circuit test, in contrast with the grid- connected temperature distribution (in Fig. 10(a)).

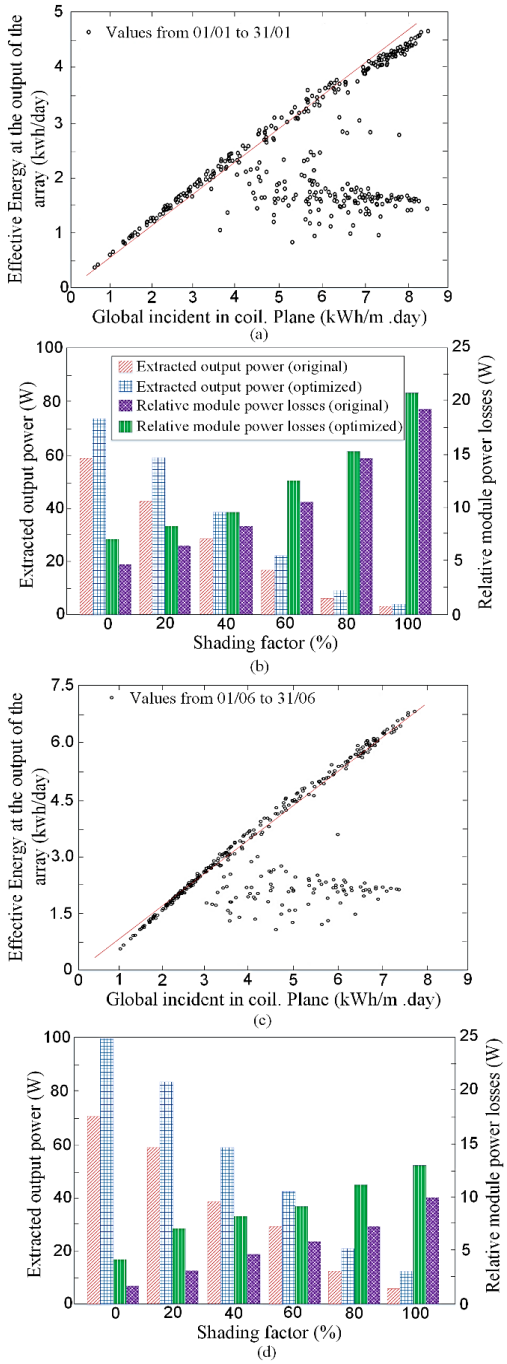

Fig. 9 Pareto-front monthly computation on the output energy of the array and its relative losses: a) effective energy at the output of the array in January, b) the extracted output power with its relative power losses in January, c) effective energy at the output of the array in June, and d) the extracted output power with its relative power losses in June

This article has been accepted for publication in a future issue of this journal, but has not been fully edited. Content may change prior to final publication. Citation information: DOI 10.1109/TSTE.2018.2849370, IEEE Transactions on Sustainable Energy

Table III. THE SIMULATION RESULTS OF 30 SQUARE-METER CELL AREA WITH *G*=1000W/ SQUARE-METER

Parameters	Pre-optimization						Post-optimization					
Average values in month of June												
Shading factors	0%	20%	40%	60%	80%	100%	0%	20%	40%	60%	80%	100%
V_{pT} [v]	0	0.197	0.252	0.622	0.832	1.038	0	0.161	0.209	0.578	0.788	0.973
GlobEff [kWh/m^2]	220.5	209.3	196.4	179.7	151.7	126.8	245.8	235.4	221.9	204.1	174.5	159.4
E_{array} [kWh]	19.72	16.55	12.87	9.91	5.65	1.32	25.97	21.43	17.51	14.13	9.77	5.52
P_{lossm} [W]	0	0.0086	0.0335	0.756	0.2199	0.2952	0	0.0069	0.0321	0.0738	0.2179	0.2935
P_o [W]	99.656	80.332	59.881	38.974	17.558	5.217	125.066	108.554	91.995	73.649	59.772	41.713
NOCT [˚C]	51.6	42.2	31.7	24.7	18.3	16.6	51.9	42.4	32.9	25.1	18.8	16.1
Average values in month of January												
V_{pT} [v]	0	0.239	0.296	0.668	0.884	1.083	0	0.177	0.227	0.596	0.806	0.994
GlobEff [kWh/m^2]	129.5	119.5	110.7	99.2	76.9	50.5	148.7	138.9	127.2	111.6	99.4	71.9
E_{array} [kWh]	14.87	12.45	10.89	9.01	7.98	5.76	25.97	21.43	17.51	14.13	9.77	5.52
P_{loss} [W]	0	0.0108	0.0354	0.781	0.2221	0.2975	0	0.0091	0.034	0.0757	0.2197	0.295
P_o [W]	74.678	58.881	37.932	21.663	6.765	2.543	98.332	79.555	59.931	44.883	21.767	13.694
NOCT [˚C]	36.8	28.7	18.8	13.8	9.8	7.5	37.2	29.2	19.5	14.2	11.1	9.4

Fig. 11 illustrates an experimental verification of the optimized values calculated in the previous section under the various shading factors of 0%, 20%, 60%, and 100% (which are observed during the whole month of June regarding Fig. 11) for G = 1000 W/m^2. During 0% shading, the blue solid curve shows the simulation results with an average value of 125.12 W, and the markers show the measured values. The blue dashed line indicates the simulation result before optimization to highlight the power improvement. At a 20% shading rate, there was a 16.53 W power reduction, shown by the solid red curve along with the experimental values (red markers) with an average of 108.56 W. The simulated values before optimization action are given by the dashed red line. For 60% shading, the green solid curve (simulated), and green markers (experimental) represent the average value of 73.55 W. In addition, a significant power maximization has been observed (nearly 35.5 W) in comparison to the green dashed line (pre-optimization) which shows 38.87 W average. Around the sunset times (18:00), when full shading condition (100%) occurs, the purple solid line (post-optimization) is verified by the purple markers. The purple dashed line presents the values (pre-optimization). A very good agreement can be seen between simulation and experimental values which highlights that the proposed optimization methodology in this research is appropriate.

Fig. 12 illustrates the experimental and simulation variation of PV module energy conversion efficiencies under different shading rates from 20-100%. Theoretically, for the single-crystalline single junction Si technology, the conversion efficiency is lower than 30%. However, the measured values at the peak operation under the irradiations of 1000 W/m^2 (during 0% shading) indicates 11.67%. During peak operation, the efficiency varies from 2.1-11.67% between 0-100% shading.

Table IV. PV SYSTEM INPUT DATA IN BARCELONA, SPAIN

Parameters	*Value*	*Unit*
Latitude	41.42	˚N
Longitude	2.13	˚E
Altitude	273	m
Orientation	SE	
Albedo	0.247	
Surface dimension	62/32	mm
Occupation ratio	89	%
Tilt angle	31	˚
Pitch length	1.51	m
Attenuation for diffuse	0.138	
Number of tested PV module	1	
Nominal output power	150	W
Maximum PV module voltage	600	V_{dc}

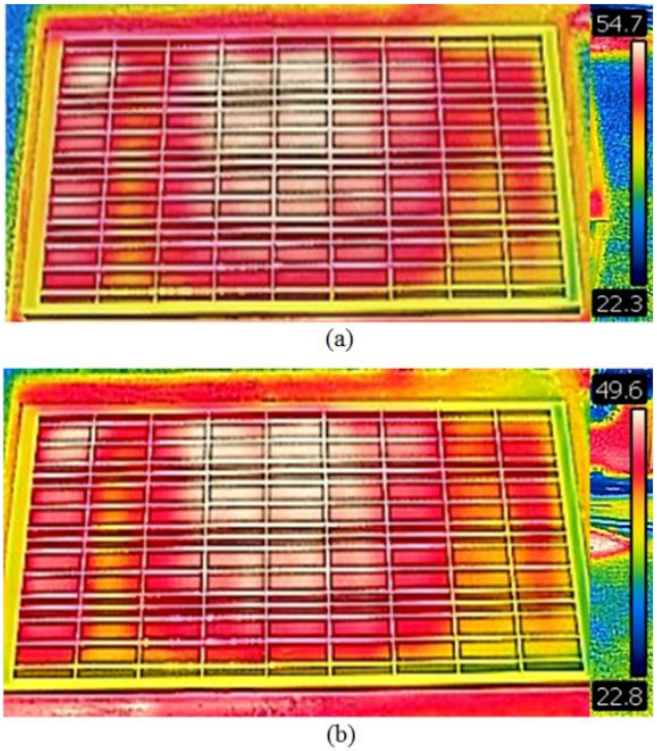

Fig. 10 IR thermo-graphs of glass/glass PV module under grid-connected condition in the open rack. a) IR thermo-graphs of glass/glass module under grid-connected, and b) and the open-circuit

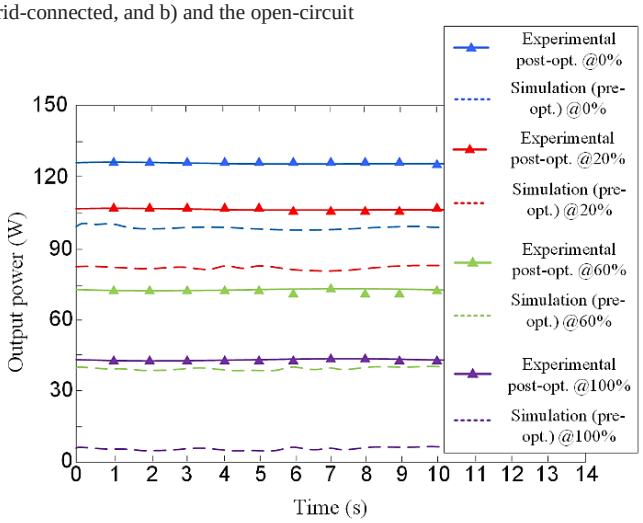

Fig. 11 The experimental output power measurement within different shading factor in June (peak time of operation)

Table V presents the annual impact of the solar PV system

This article has been accepted for publication in a future issue of this journal, but has not been fully edited. Content may change prior to final publication. Citation information: DOI 10.1109/TSTE.2018.2849370, IEEE Transactions on Sustainable Energy

optimization over different shading rates from 0% (no shading) to 100% with an average of 3 kg/ year CO_2 emissions reduction which translates to a saving of $84,000 (USD) per ton CO_2. Based on the table, the environmental issues of the project have been considered to reduce CO_2 emissions as a part of green power generation projects.

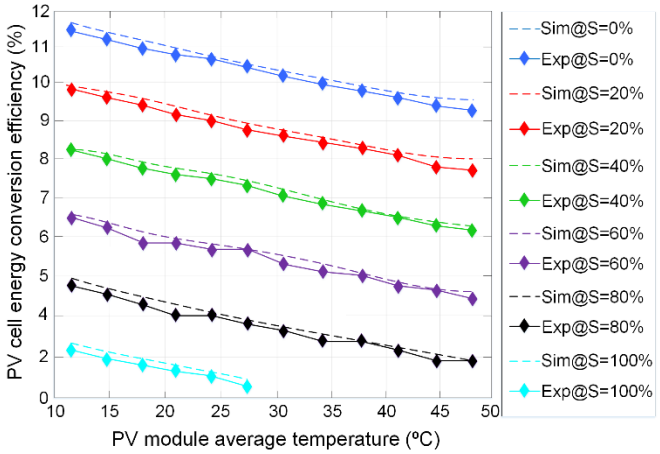

Fig. 12 Measured PV cell efficiencies under different shading rates

Table V. REDUCED CO_2 / EACH 100 W POWER GENERATION

Shading rate/ model	*Unit*	*Pre-opt*	*Post-opt*
0%	kg	29.8	32.7
20%	kg	24.6	27.8
40%	kg	17.6	20.5
60%	kg	12.2	15.5
80%	kg	8.8	11.3
100%	kg	3.6	6.4

VI. CONCLUSION

The research proposes a 3-D Pareto optimization methodology using a window-zoom-in approach to maximize a PV array's effective output energy while considering complete and partial shading of the PV array in an urban environment. The proposed methodology ensures special attention to the input data of the PV module as it has a considerable effect on the outputs. A number of significant input parameters such as NOCT, weather, and sky condition (clouds) were carefully considered. Moreover, the PV system was coupled with an enhanced MPPT controller, which uses an advanced P&O algorithm. The design variables were modified by the dual-level ANOVA method to find the optimized values over tens of simulations. The simulation results are presented for the original and optimized variables to highlight the design improvement particularly the output power. The analytical and numerical parts of the study have been successfully verified and show a good agreement with an experimental investigation where a smaller scale of the whole system with maximum efficiency of 11.67% (60 cells) was tested in Barcelona city, Spain. The proposed optimization technique was employed for the photovoltaic system design and optimization, where the nominal power generation of 6 kW was targeted for a complex structure in the urban environment. Annual reduced CO_2 emissions using optimized model for each 100 W is 3 kg which saved thousands of US dollars per year.

V. REFERENCES

[1] T. S. Babu, and *et al*., "Particle Swarm Optimization Based Solar PV Array Reconfiguration of the Maximum Power Extraction Under Partial Shading Conditions," *IEEE Trans. on Sustainable. Energy*, Vol. 9, No. 1 pp.74-85, Jan. 2018.

[2] A. Xenophontos, and A. M. Bazzi, "Model-Based Maximum Power Curves of Solar Photovoltaic Panels Under Partial Shading Conditions," *IEEE Trans. Of Photovoltaics*, Vol. 8, No. 1, pp. 223-229, Jan. 2018.

[3] Z. Zhen, X. Taoyun, S. Yanping, L. Wang, P. Jia and J. Yu, "A Method to Test Operating Cell Temperature for BIPV Modules," *IEEE Trans. Of Photovoltaics*, Vol. 6, No. 1 pp.272-277, Jan. 2016.

[4] N. Belhaouas, M.-S. A. Cheikh, P. Agathoklis, M.-R. Oularbi, B. Amrouche, K. Sedraoui, and N. Djilali, "PV array power output maximization under partial shading using new shifted PV array arrangements," *Applied Energy Journal*, Vol. 187, pp. 326-337, Feb. 2017.

[5] R. Rachchh, M. Kumar, and B. Tripathi, "Solar photovoltaic system design optimization by shading analysis to maximize energy generation from limited urban area," *Energy Conversion and Management, Journal*, Vol. 115, pp. 244-252, May 2016.

[6] M. Khoroshiltseva, D. Slanzi, and I. Poli, "A Pareto-based multi-objective optimization algorithm to design energy-efficient shading devices," *Applied Energy Journal*, Vol. 184, pp. 1400-1410, Dec. 2016.

[7] A. J. Hanson, and et al., "Partial-Shading Assessment of Photovoltaic Installations via Module-Level Monitoring," *IEEE Trans. Of Photovoltaics*, Vol. 4, No. 6, pp. 1618-1624, Nov. 2014.

[8] F. Belhachat, and C. Larbes, "Modeling, analysis and comparison of solar photovoltaic array configurations under partial shading conditions," *Solar Energy Journal*, Vol. 120, pp. 399-418, Aug. 2015.

[9] A. Fathy, "Reliable and efficient approach for mitigating the shading effect on photovoltaic module based on Modified Artificial Bee Colony algorithm," *Renewable Energy Journal*, Vol. 81, pp. 78-88, Sep. 2015.

[10] M Holt, "NEC REQUIREMENTS FOR SOLAR PHOTOVOLTAIC SYSTEMS," *Chapter book*, ISBN: 9780986353444, pp. 1-608, 2017.

[11] S. Mohanty, B. Subudhi, and P. Kumar Ray, "A Grey Wolf-Assisted Perturb & Observe MPPT Algorithm for a PV System," *IEEE Trans. on Energy Conversion*, Vol. 32, No. 1 pp.272-277, March. 2017.

[12] A. A. Elbaset, H. Ali, M. Abd-El Sattar, and M. Khaled, "Implementation of a modified perturb and observe maximum power point tracking algorithm for photovoltaic system using an embedded microcontroller," *IET Renewable Power Generation*, Vol. 10, No. 4, pp. 551–560, 2016.

[13] X. Li, and et al., "Modified Beta Algorithm for GMPPT and Partial Shading Detection in Photovoltaic Systems," *IEEE Trans. On Power Electronics*, Vol. 33, No. 3, pp. 2172-2182, March. 2018.

[14] J. Ahmed, and Z. Salam, "An Accurate Method for MPPT to Detect the Partial Shading Occurrence in a PV System," *IEEE Trans. On Ind. Informatics*, Vol. 13, pp. 2151-2161, Oct. 2017.

[15] A. M. S. Furtado, and *et al*., "A Reduced Voltage Range Global Maximum Power Point Tracking Algorithm for Photovoltaic Systems Under Partial Shading Conditions," *IEEE Trans. On Ind. Informatics*, Vol. 65, No. 4, pp. 3252-3253, Apr. 2018.

[16] K. Ishaque, Z. Salam, A. Shamsudin, M. Amjad, "A direct control based maximum power point tracking method for photovoltaic system under partial shading conditions using particle swarm optimization algorithm," *Applied Energy Journal*, Vol. 99, pp. 414-422, Nov. 2012.

[17] K. Wang, Y-L. He, X-D. Xue, B-C. Du, "Multi-objective optimization of the aiming strategy for the solar power tower with a cavity receiver by using the non-dominated sorting genetic algorithm," *Applied Energy, Journal*, Vol. 205, pp. 399-416, Nov. 2017.

[18] N. N. Castellano, J. Antonio G. Parra, J. V-Guirado, and F. M-Agugliaro, "Optimal displacement of photovoltaic array's rows using a novel shading model," *Applied Energy Journal*, Vol. 144, pp. 1-9, April. 2015.

[19] P. Asef, R. Bargallo, M. R. Barzegaran, A. Lapthorn, and D. Mewes, "Multi-objective Design Optimization Using Dual-Level Response Surface Methodology and Booth's Algorithm for Permanent Magnet Synchronous Generators," *IEEE Trans. on Energy Conversion*, Vol. PP, No. 99, pp.1-8, Nov. 2017